NANO LETTERS

Letter

pubs.acs.org/NanoLett

The Spatial Resolution Limit for an Individual Domain Wall in Magnetic Nanowires

Sumit Dutta,[†,#] Saima A. Siddiqui,[†,#] Jean Anne Currivan-Incorvia,[‡] Caroline A. Ross,[*,§] and Marc A. Baldo[*,†]

[†]Department of Electrical Engineering and Computer Science, [§]Department of Materials Science and Engineering, Massachusetts Institute of Technology, Cambridge, Massachusetts 02139, United States

[‡]Department of Physics, Harvard University, Cambridge, Massachusetts 02138, United States

Supporting Information

ABSTRACT: Magnetic nanowires are the foundation of several promising nonvolatile computing devices, most notably magnetic racetrack memory and domain wall logic. Here, we determine the analog information capacity in these technologies, analyzing a magnetic nanowire containing a single domain wall. Although wires can be deliberately patterned with notches to define discrete positions for domain walls, the line edge roughness of the wire can also trap domain walls at dimensions below the resolution of the fabrication process, determining the fundamental resolution limit for the placement of a domain wall. Using a fractal model for the edge roughness, we show theoretically and experimentally that the analog information capacity for wires is limited by the self-affine statistics of the wire edge roughness, a relevant result for domain wall devices scaled to regimes where edge roughness dominates the energy landscape in which the walls move.

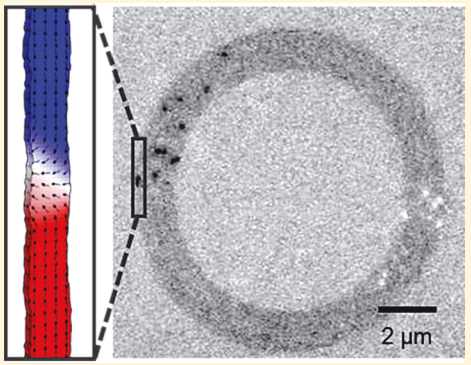

KEYWORDS: *Fractals, line edge roughness, magnetic nanowires, domain walls, magnetic force microscopy*

The position of a magnetic domain wall within a nanowire can be used as an information token in spintronic memory and logic devices.[1−4] At high information densities, when the width of a magnetic nanowire is below 100 nm, domain walls are increasingly influenced by inhomogeneities at the edges of the wire.[6−8] In the presence of edge roughness, domain walls within narrow wires relax into constrictions in the wire to lower their total energy.[5] However, it remains unclear how the statistical properties of nanowire edge roughness quantize the position of the domain wall along the wire, thereby determining the fundamental spatial resolution limit (i.e., the density of possible locations for a single domain wall at remanence) for this spintronic technology.

Like all fabricated structures, the intrinsic line edge roughness of nanowires is statistically self-affine.[10−12] In general, edges are self-affine if they look smooth over large length scales, but close-up, appear like the coastlines familiar from fractals.[11,13] The transition between the smooth and the rough length scales is defined by the correlation length, ξ, a property of the particular fabrication process used to make the wires. The central result of this work is that the correlation length determines the spatial quantization in the wire because it is the shortest length scale before the amplitude of the edge roughness begins to decrease at finer resolution.[10,14,15] Thus, the coastline of the wire can be understood as a series of harbors of width $\sim\xi$. Each harbor contains finer edge roughness, but if the domain wall width is smaller than ξ, then each harbor roughly corresponds to a single dominant trap site for a domain wall. As a consequence, for devices that rely on the location of a domain wall to, for example, store data, there is an inherent limit on the precision with which an individual domain wall can be placed. (We consider a single domain wall here, and do not consider the behavior of multiple interacting domain walls.) Although prior work has shown that notches or constrictions act as traps, this work shows that the natural self-affine roughness also produces traps and that the statistics of such traps differ qualitatively from that of a wire with random edge roughness.

To analyze the impact of edge roughness, we fabricate magnetic nanowires, characterize their edge profiles, and compare to self-affine fractal models. Previously, the Weierstrass−Mandelbrot (WM) model has been used to describe the edges of wires, such as those of antennas.[11] The edge deviation Δy as a function of the position x along the wire length is given by the WM model in one dimension:

$$\Delta y(x) = B_{\mathrm{LER}} \sum_{p=1}^{\infty} C_p \nu^{-pH_Q} \sin\left[\frac{2\pi}{\xi}\nu^p(x\cos\Psi_p) + \Phi_p\right] \quad (1)$$

The WM model is appropriate to model a self-affine wire because it starts with a sinusoid with an amplitude B_{LER}, defined by the line edge roughness of our fabricated wires, and a period

Received: July 27, 2017
Published: August 16, 2017

DOI: 10.1021/acs.nanolett.7b03199
Nano Lett. 2017, 17, 5869−5874

ξ, defined by the correlation length. Then, additional higher-frequency modes are added, with decreasing amplitude and increasing spatial frequency. The Hurst exponent, H_Q = 0.3, and the seed of the geometric progression that accounts for spectral separation, ν = 1.5, are empirical parameters taken from the antenna model in ref 9. H_Q represents how much weaker higher frequency modes become. Since ν is not unity, the spatial frequency of higher modes increases nonlinearly rather than as integer multiples like harmonics. Furthermore, the amplitudes C_p of each mode are randomized with a Gaussian distribution with zero mean and a standard deviation of 1, and the phases Ψ_p and Φ_p of each mode are randomized with a uniform distribution on $[-\pi, \pi]$.

Figure 1a–c shows scanning electron micrographs of Co wires with in-plane magnetic anisotropy (IMA), fabricated in

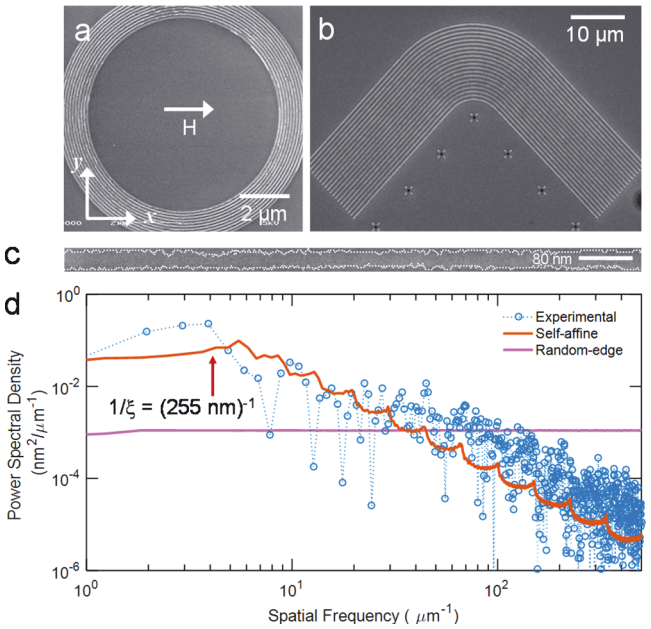

Figure 1. Scanning electron microscope (SEM) images of (a) concentric rings and (b) L-shaped nanowires. (c) SEM image of part of L-shaped wire discretized as shown by the dotted line. (d) Power spectral density of the line edge roughness of the discretized wire, the average of 10^4 synthesized self-affine wires, and the average of 10^4 synthesized random-edge wires. The correlation length, ξ, is extracted from the discretized wire and is applied to synthesize the self-affine wires.

the shape of concentric rings, L's, and straight lines, respectively, with an average width of 80 nm and thickness of 5 nm.[16] The power spectral density (PSD) of line edge roughness in the measured wires is shown in Figure 1d. Straight lines such as Figure 1c are characterized to extract the parameters: B_{LER} = 2 nm and ξ = 255 nm, as determined from the knee of the PSD at $1/\xi$.[17] The concentric ring nanowires exhibit similar edge roughness, but longer correlation lengths of ξ = 0.99 μm.

For comparison with the experimentally determined edge roughness distribution of the Co wires, we numerically synthesize wires with self-affine statistics using eq 1. In addition, we synthesize wires with a random-edge profile, where the edge deviation of each edge cell is randomly assigned a value between −6 and 6 nm with a uniform distribution. Good agreement is found between the PSD of the self-affine wires and the experimental wires, but the random-edge wires clearly diverge from the characteristics of real wires. This contrast highlights the key role of self-affine statistics suppressing roughness at short length scales in real wires, for which random roughness is a poor approximation.

The edge roughness of the wires leads to a variation in the total energy of a domain wall as a function of distance along the wire, with the consequence that a domain wall will be trapped at certain locations as it moves along the wire in response to a magnetic field. To determine the distribution of domain-wall trap sites and relate domain wall traveling distances to the applied field, we use micromagnetic models of 60-nm-wide, 5-nm-thick Co wires with self-affine or random-edge roughness, discretized by the cell size of 3 × 3 × 2.5 nm^3. The Co has random magnetocrystalline anisotropy, and its remanent magnetization configuration is dominated by shape anisotropy, leading to IMA. For this wire geometry, the domain walls are transverse walls with core magnetization lying in plane, transverse to the length of the wire, and the domain wall width is similar to the wire width. Typical domain wall configurations are shown in Figure S3.

A single domain wall is placed at a specific location along a wire and then allowed to relax at zero field with its final position recorded; this is repeated for all possible starting locations along the wire. Figure 2a shows the initial and final

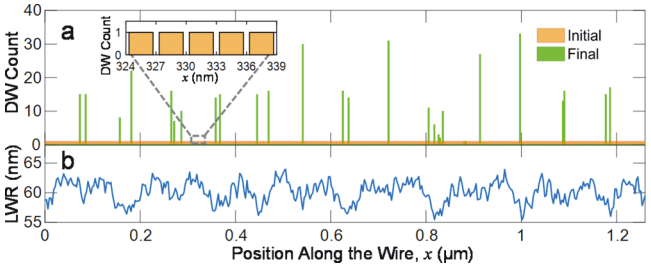

Figure 2. (a) Final positions into which domain walls relax from their initial positions of domain wall nucleation, for one wire in micromagnetic simulations. The bin width is chosen to be the size of one simulation cell, 3 nm. Inset: Zoom in view of initial positions. (b) Line width roughness profile of the wire shows that the traps often correspond to local minima in width.

domain wall positions for one wire, indicating that there are specific pinning sites or traps along the wire (Figure 2b) to which the domain wall is attracted. These are typically locations of local minima in the wire width at which the energy of the domain wall is minimized.

We define Δx to be the distance from one discrete domain wall trap to the next one along the wire. In other words, the Δx values are the distances between the discrete domain wall traps in Figure 2a. Figure 3a shows the distribution of spacing between domain wall traps in simulations of 41 synthetically generated self-affine wires with ξ = 255 nm. There is a peak, Δx_0, for self-affine wires at 85 nm ≈ $\xi/3$. Δx_0 defines the distance of the first strong trap from the initial position of the domain walls. Note that the distribution is nonuniform. The mean Δx_μ = 125 nm and the standard deviation Δx_σ = 77 nm.

In simulations of 30 self-affine wires with a shorter correlation length ξ = 127 nm, we find Δx_0 = 54 nm, showing that Δx_0 decreases with decreasing ξ. In 30 wires with a random-edge profile, the Δx distribution shows that domain wall traps are more likely to be spaced closely together. This is

DOI: 10.1021/acs.nanolett.7b03199
Nano Lett. 2017, 17, 5869–5874

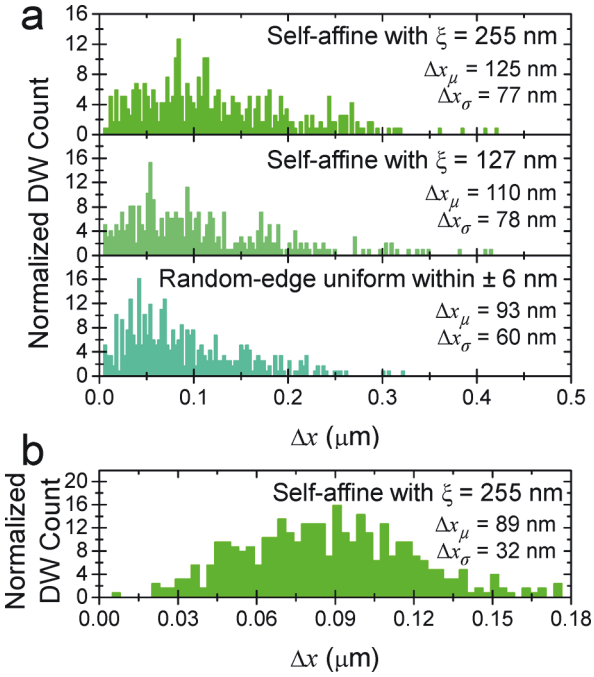

Figure 3. Distribution of spacing Δx between domain wall discrete positions for (a) IMA and (b) PMA wires, including wires with self-affine edge profiles with correlation length ξ and wires with random-edge profiles. The distributions are normalized by area.

consistent with the higher amplitude of roughness at short length scales in a random-edge wire.

In contrast, domain walls are narrower in wires with perpendicular magnetic anisotropy (PMA).[7,8] In Figure 3b, we simulate 30 CoFeB wires with PMA. As in the IMA simulations, we find that domain walls relax to positions distributed at discrete locations along the wire. The standard deviation of the trap locations is less than that found in the IMA Co wire simulations since the narrow PMA domain walls interact more strongly with high-frequency roughness. We further observe strong anticorrelations between the pinning sites, suggesting that the self-affine edge roughness statistics manifest similarly in PMA and IMA.

The information density of a nanowire, that is, the number of distinct possible locations for a domain wall, is determined from the average spacing between domain wall traps. We find from Figure 3 that, when ξ = 255 nm, the information density of IMA wires is $1/\Delta x_\mu \sim 10$ positions/μm and that of PMA wires is $1/\Delta x_\mu \sim 14$ positions/μm. These results are expected to scale with the reciprocal of the correlation length, $1/\xi$, and consequently the attainable information density fundamentally depends on the resolution of the fabrication process as long as the domain wall width is smaller than ξ. Notably, the maximum spatial resolution is below the correlation length. Thus, the natural edge roughness of a nanowire yields a statistically higher information density than any fabricated pattern.

After identifying the zero-field pinning sites in self-affine nanowires, we apply steady-state magnetic fields to move the domain walls along 1500 micromagnetic models of synthetic IMA wires. A domain wall is initialized in a trap on one end of each wire, and the traveling distance of the domain wall to its final position is then calculated after applying the field. Figure 4 shows the histograms of the distances traveled by domain walls from an initial trap to a final trap, under four different steady-state magnetic field values. We do not perform this simulation

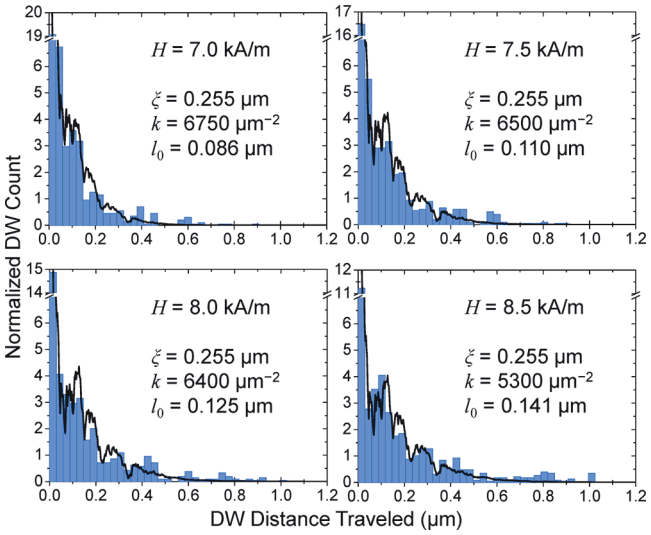

Figure 4. Distributions of distances traveled by domain walls in simulated nanowires. The sample size is 1500 wires. The fractal analytical model is the overlaid line with parameters listed for each applied field.

in PMA because domain walls have a high critical field for motion and as such operate only in the precessional regime above Walker breakdown and are completely detrapped, that is, once they start moving they continue until the end of the wire.[7]

A similar procedure was conducted experimentally using the lithographically patterned Co wires. We apply steady-state magnetic fields and measure the distance traveled by domain walls in Co wires using magnetic force microscopy. Figure 5 shows our experimental results, including the magnetic force micrographs of the nanowire rings after applying different magnetic fields along the wires. The head-to-head and tail-to-tail transverse domain walls show as bright or dark contrast, respectively.

We propose an analytical model for the distribution of the propagation distances of domain walls when applying a steady-state magnetic field H:

$$\frac{df}{dx} = \left(-\frac{1}{l_0} + k\Delta y(x - x_{\min})\right)f \tag{2}$$

Here, $\Delta y(x)$ is the edge profile, e.g., from the WM model in eq 1, and f is the fraction of domain walls that are still propagating at distance x. We define $x = 0$ to be the initial position of each domain wall, and $x_{\min}$ is the value of x at the minimum of $\Delta y(x)$ within $0 < x < 1$ μm. The fit parameters, k and l_0, account for the effects on trapping probability that are dependent and independent of edge roughness, respectively. The fit parameter, k, weights the significance of trapping due to edge roughness. In contrast l_0 characterizes all spatially independent sources of pinning, such as the effect of fluctuations in the magnetic anisotropy within the microstructure.[18] The in-plane grain size of the film is ~5−10 nm, leading to local fluctuations in anisotropy on a length scale much smaller than ξ. The surface roughness of <0.2 nm is not expected to lead to significant pinning.

Equation 2 is solved in the Supporting Information; see eq S2. The solution is a function of random variables; thus for fitting purposes we determine $(-df/dx)_{\text{mean}}$, the average of $(-df/dx)$ for N = 1500 wires. In Figure 4 and Figure 5b, $(-df/dx)_{\text{mean}}$ is fitted to the distributions of distances traveled by

DOI: 10.1021/acs.nanolett.7b03199
Nano Lett. 2017, 17, 5869−5874

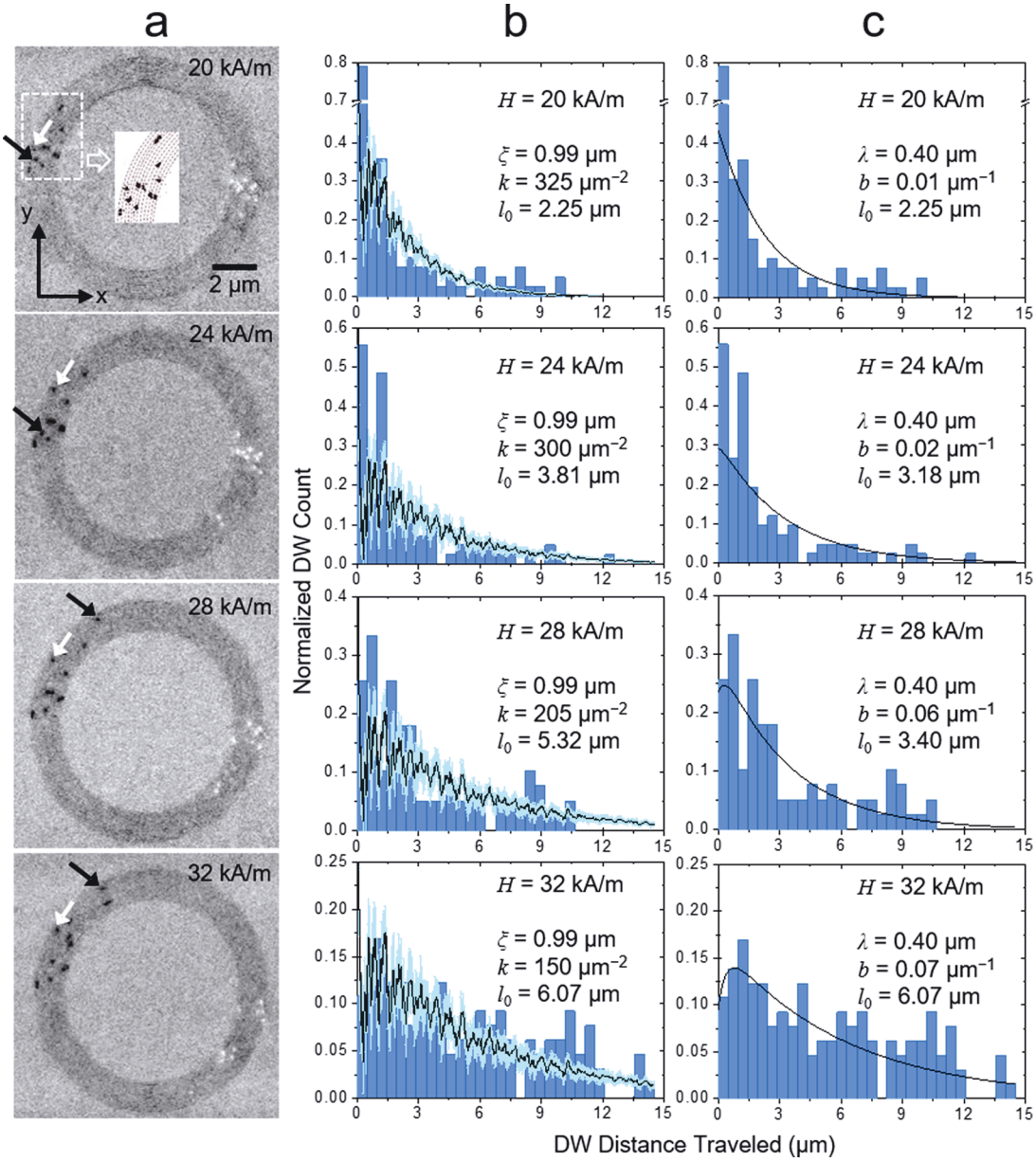

Figure 5. (a) Magnetic force microscopy images of domain walls in concentric rings with applied magnetic fields of 20, 24, 28, and 32 kA/m along the *y*-axis. The black and the white dots represent the tail-to-tail and head-to-head domain walls, respectively. The white and the black arrows in each image show the position of two tail-to-tail domain walls in the second and third rings (from outside), respectively. The inset in the top image shows a thresholded rendering of the image in which the tail-to-tail domain walls show clearly. The nanowires are marked by the red dotted lines. (b) Fractal analytical model and (c) exponential analytical model overlaid on distributions of distances traveled by domain walls in experiment. The sample size is 94, 94, 83, and 134 wires in increasing order of applied fields.

domain walls in IMA Co wires found in both simulation and experiment, respectively.

The analytical model parameters, l_0 and k, obtained from fits to the simulation data, are listed in Figure 4. As expected, l_0 increases with increasing H since domain walls move farther at higher fields before encountering a trap that can prevent further motion. The fit between $(-df/dx)_{mean}$ and the experimental data in Figure 5b also shows an increase in l_0 with field. The parameter k decreases with increasing H in fits to both simulation and experimental data. We find that $\xi = 0.99$ μm in the analytical model fits the experimental data well, where $\xi = 0.99$ μm is the correlation length extracted from the PSD of the concentric ring wires (Figure 1a) from which the domain wall displacements up to 2.5 μm were measured.

As shown in Figure 4, the simulations and analytic model for domain wall propagation in nanowires with self-affine edge profiles show oscillations in trapping probability over distances equivalent to multiple correlation lengths. The strongest impact of edge roughness, however, occurs within the first correlation length. Under this approximation, we can then simplify the analytic model of eq 2 to the width-independent term, $-1/l_0$, and a width-dependent exponentially decaying autocorrelation term:

$$\frac{df}{dx} = \left(-\frac{1}{l_0} + b\,\exp(-x/\lambda)\right) f \tag{3}$$

DOI: 10.1021/acs.nanolett.7b03199
Nano Lett. 2017, 17, 5869−5874

This model, eq 3, is solved in the Supporting Information. We fit this simplified model in eq S4 to the experimental data in Figure 5c. We choose $\lambda = 0.4\xi$ because the distance to the first trap can be approximated by Δx_0, which is roughly $\xi/3$ and 0.45ξ in Figure 3, for $\xi = 255$ and 127 nm, respectively. In the fit in Figure 5c, ξ remains the same as in Figure 5b, l_0 has values similar to those in Figure 5b and also increases with H. The fit constant b represents the weight of the exponentially decaying term corresponding to line edge roughness. We have sufficient experimental data and resolution in the magnetic force micrographs to group the propagation distances into 0.5-μm-wide bins. Given this constraint, we require higher fields such that $l_0 \gg 0.5$ μm to image any effects of roughness. Indeed, the simplified model of eq 3 diverges from an exponential decay with $b > 0$, as observed in the highest field case of $H = 32$ kA/m, meaning that $b > 0$ when there is at least enough energy to move domain walls beyond the first trap, confirming the effect of edge roughness in these wires.

In conclusion, we study nanowires in the regime where the magnetic domain wall width is smaller than the self-affine correlation length ξ of the wire edge roughness. We find a discrete distribution of domain wall traps. The maximum density of locations at which a domain wall can be found at remanence is observed in the peak of Δx distributions and is found to be below ξ. This determines how many possible domain wall locations are present, that is, the density of traps along the wire, and therefore fundamentally limits the placement accuracy of a domain wall in a wire. For a representative correlation length of $\xi = 255$ nm, the density of traps in PMA wires (14 positions/μm) is higher than that of IMA wires (10 positions/μm) for the same wire width.

When domain walls are moved by a magnetic field or current, the distribution of their distance traveled can be modeled analytically by eq 2, whose width-independent component creates the shape of an exponential decay with increasing distance and whose width-dependent component is based on the edge deviation fractal model. Our wire edge model applies to narrower wires, considering that the root-mean-square edge roughness does not decrease in narrower wires.[16] Notches with a higher pinning potential than that derived from line edge roughness may be introduced for predictable control, but at the cost of decreasing the maximum density of pinning sites. These results are relevant to the scaling performance of domain wall devices into regimes where line edge roughness dominates the energy landscape in which the walls move. Furthermore, similar limits to information capacity are expected to apply to a wider class of domain wall nanoelectronics, such as ferroelectric devices.[19]

■ ASSOCIATED CONTENT

Supporting Information

The Supporting Information is available free of charge on the ACS Publications website at DOI: 10.1021/acs.nanolett.7b03199.

Experimental details (PDF)

■ AUTHOR INFORMATION

Corresponding Authors

*E-mail address: (M. A. Baldo) baldo@mit.edu.
*E-mail address: (C. A. Ross) caross@mit.edu.

ORCID

Sumit Dutta: 0000-0002-2766-8516

Author Contributions

#S.D. and S.A.S. contributed equally to this work. S.D. developed the theoretical analysis, conducted the micromagnetic simulations, and assisted with data analysis. S.A.S. designed the experiment and performed nanofabrication, measurements, and experimental data analysis. J.A.C.-I. assisted with fabrication. C.A.R. and M.A.B. supervised the design of experiments, planning of the project, and contributed to the analysis.

Notes

The authors declare no competing financial interest.

■ ACKNOWLEDGMENTS

S.D. thanks D. I. Paul for discussion. This project was supported by the National Science Foundation award 1639921 and the Nanoelectronics Research Corporation, a subsidiary of the Semiconductor Research Corporation, through Memory, Logic, and Logic in Memory Using Three Terminal Magnetic Tunnel Junctions, an SRC-NRI Nanoelectronics Research Initiative under Research Task ID 2700.002.

■ ABBREVIATIONS

IMA, in-plane magnetic anisotropy; PMA, perpendicular magnetic anisotropy; PSD, power spectral density; SEM, scanning electron microscope

■ REFERENCES

(1) Parkin, S. S. P.; Hayashi, M.; Thomas, L. *Science* **2008**, *320*, 190−194.
(2) Jiang, X.; Thomas, L.; Moriya, R.; Parkin, S. S. P. *Nano Lett.* **2011**, *11*, 96−100.
(3) Currivan, J. A.; Jang, Y.; Mascaro, M. D.; Baldo, M. A.; Ross, C. A. *IEEE Magn. Lett.* **2012**, *3*, 3000104.
(4) Currivan-Incorvia, J. A.; Siddiqui, S. A.; Dutta, S.; Evarts, E. R.; Zhang, J.; Bono, D.; Ross, C. A.; Baldo, M. A. *Nat. Commun.* **2016**, *7*, 10275.
(5) Hayashi, M.; Thomas, L.; Rettner, C.; Moriya, R.; Parkin, S. S. P. *Nat. Phys.* **2007**, *3*, 21−25.
(6) Huang, X. P.; Shi, Z. L.; Wang, M.; Konoto, M.; Zhou, H. S.; Ma, G. B.; Wu, D.; Peng, R.; Ming, N. B. *Adv. Mater.* **2010**, *22*, 2711.
(7) Dutta, S.; Siddiqui, S. A.; Currivan-Incorvia, J. A.; Ross, C. A.; Baldo, M. A. *AIP Adv.* **2015**, *5*, 127206.
(8) Koyama, T.; Chiba, D.; Ueda, K.; Kondou, K.; Tanigawa, H.; Fukami, S.; Suzuki, T.; Ohshima, N.; Ishiwata, N.; Nakatani, Y.; Kobayashi, K.; Ono, T. *Nat. Mater.* **2011**, *10*, 194.
(9) O'Brien, L.; Petit, D.; Lewis, E. R.; Cowburn, R. P.; Read, D. E.; Sampaio, J.; Zeng, H. T.; Jausovec, A.-V. *Phys. Rev. Lett.* **2011**, *106*, 087204.
(10) Palasantzas, G. *Phys. Rev. B: Condens. Matter Mater. Phys.* **1993**, *48*, 14472.
(11) Pike, R.; Sabatier, P. *Scattering: scattering and inverse scattering in pure and applied science*; Academic Press: Cambridge, MA, 2002.
(12) Urbach, J. S.; Madison, R. C.; Markert, J. T. *Phys. Rev. Lett.* **1995**, *75*, 276−279.
(13) Majumdar, A.; Tien, C. L. *Wear* **1990**, *136*, 313−327.
(14) Hiraiwa, A.; Nishida, A. *J. Vac. Sci. Technol., B: Nanotechnol. Microelectron.: Mater., Process., Meas., Phenom.* **2010**, *28*, 1132−1137.
(15) Moktadir, Z.; Darquié, B.; Kraft, M.; Hinds, E. A. *J. Mod. Opt.* **2007**, *54*, 2149−2160.
(16) Currivan, J. A.; Siddiqui, S. A.; Ahn, S.; Tryputen, L.; Beach, G. S. D.; Baldo, M. A.; Ross, C. A. *J. Vac. Sci. Technol., B: Nanotechnol. Microelectron.: Mater., Process., Meas., Phenom.* **2014**, *32*, 021601.
(17) Ji, H.; Robbins, M. O. *Phys. Rev. B: Condens. Matter Mater. Phys.* **1992**, *46*, 14519.

DOI: 10.1021/acs.nanolett.7b03199
Nano Lett. 2017, 17, 5869−5874

(18) Zhang, J.; Siddiqui, S. A.; Ho, P.; Currivan-Incorvia, J. A.; Tryputen, L.; Lage, E.; Bono, D. C.; Baldo, M. A.; Ross, C. A. *New J. Phys.* **2016**, *18*, 053028.
(19) McGilly, L. J.; Yudin, P.; Feigl, L.; Tagantsev, A. K.; Setter, N. *Nat. Nanotechnol.* **2015**, *10*, 145−150.

DOI: 10.1021/acs.nanolett.7b03199
Nano Lett. 2017, 17, 5869−5874